Biochimica et Biophysica Acta 1848 (2015) 1294–1302

Contents lists available at ScienceDirect

Biochimica et Biophysica Acta

journal homepage: www.elsevier.com/locate/bbamem

Solution structure of the transmembrane 2 domain of the human melanocortin-4 receptor in sodium dodecyl sulfate (SDS) micelles and the functional implication of the D90N mutant

Ji-Hye Yun [a], Minsup Kim [c], Kuglae Kim [b], Dongju Lee [a], Youngjin Jung [a], Daeseok Oh [a], Yoon-Joo Ko [d], Art E. Cho [c], Hyun-Soo Cho [b], Weontae Lee [a,*]

[a] Department of Biochemistry, College of Life Science and Biotechnology, Yonsei University, Seoul 120-749, Republic of Korea
[b] Department of Systems Biology, College of Life Science and Biotechnology, Yonsei University, Seoul 120-749, Republic of Korea
[c] Department of Bioinformatics, Korea University, Sejong 136-701, Republic of Korea
[d] National Center for Inter-University Research Facilities, Seoul National University, Seoul 151-747, Republic of Korea

ARTICLE INFO

Article history:
Received 13 October 2014
Received in revised form 3 February 2015
Accepted 27 February 2015
Available online 6 March 2015

Keywords:
Melanocortin receptor
Obesity
Transmembrane domain
Nuclear magnetic resonance spectroscopy
Sodium allosteric binding

ABSTRACT

The melanocortin receptors (MCRs) are members of the G protein-coupled receptor (GPCR) 1 superfamily with seven transmembrane (TM) domains. Among them, the melanocortin-4 receptor (MC4R) subtype has been highlighted recently by genetic studies in obese humans. In particular, in a patient with severe early-onset obesity, a novel heterozygous mutation in the MC4R gene was found in an exchange of Asp to Asn in the 90th amino acid residue located in the TM 2 domain ($MC4R^{D90N}$). Mutations in the MC4R gene are the most frequent monogenic causes of severe obesity and are described as heterozygous with loss of function. We determine solution structures of the TM 2 domain of MC4R ($MC4R^{TM2}$) and compared secondary structure of Asp90 mutant ($MC4R^{TM2\text{-}D90N}$) in a micelle environment by nuclear magnetic resonance (NMR) spectroscopy. NMR structure shows that $MC4R^{TM2}$ forms a long α-helix with a kink at Gly98. Interestingly, the structure of $MC4R^{TM2\text{-}D90N}$ is similar to that of $MC4R^{TM2}$ based on data from CD and NMR spectrum. However, the thermal stability and homogeneity of $MC4R^{D90N}$ is quite different from those of MC4R. The structure from molecular modeling suggests that $Asp90^{2.50}$ plays a key role in allosteric sodium ion binding. Our data suggest that the sodium ion interaction of $Asp90^{2.50}$ in the allosteric pocket of MC4R is essential to its function, explaining the loss of function of the $MC4R^{D90N}$ mutant.

1. Introduction

G-protein-coupled receptors (GPCRs) are the largest and most diverse family of membrane proteins in eukaryotes, which regulate diverse biological and physiological processes through orthosteric and allosteric ligand interaction. The melanocortin receptor (MCR) system consists of five receptor subtypes (MC1R–MC5R) and belongs to the superfamily of Class A GPCRs. The MCRs play an important role in skin pigmentation [1], adrenocortical function [1], energy homeostasis [2,3], feeding behavior [4,5], sexual function [6], and exocrine gland function. The MC4R, expressed predominantly in the brain, has been considered as an obesity drug target [7,8]. It is activated by agonists such as proopiomelanocortin (POMC)-derived peptides and coupled to the Gs protein and adenylyl cyclase to negatively regulate food intake [6,9]. In general, heterozygous and homozygous mutants of GPCR are involved in a loss of function in terms of Gs/adenylyl cyclase activation and intracellular retention by GPCR mutants. Recently, a number of reports have demonstrated that heterozygous and homozygous mutation of MC4R is a critical factor in the regulation of food uptake as well as obesity [5,10–13].

Various homozygous and heterozygous mutants of MC4R have been identified: null mutants, intracellular trapped mutants, binding-defective mutants, and signaling-defective mutants [10,14–18]. Among them, the heterozygous D90N mutant of MC4R ($MC4R^{D90N}$) has been identified as a signaling-defective mutant, which is expressed on the cell surface with normal ligand binding affinity. Asp90 residue in the transmembrane (TM) 2 domain of MC4R ($MC4R^{TM2}$) is highly conserved in all MCRs, and its mutation induces hetero-dimerization with wild-type MC4R, blocking MC4R–G protein interaction. Asp90 residue of $MC4R^{TM2}$ ($Asp90^{2.50}$) is mostly conserved in numerous Class A GPCRs by the Ballesteros–Weinstein numbering method [19]. Previous mutagenesis studies have reported that the mutation of

Abbreviations: MCR, melanocortin receptor; hMC4R, human melanocortin 4 receptor; MSH, melanocyte stimulating hormone; NMR, nuclear magnetic resonance; NOE, nuclear Overhauser effect

* Corresponding author at: Department of Biochemistry, College of Life Science and Biotechnology, Yonsei University, Seodaemoon-Gu, Shinchon-dong 134, Seoul 120-749, Republic of Korea. Tel.: +82 2 2123 2706; fax: +82 2 363 2706.
E-mail address: wlee@spin.yonsei.ac.kr (W. Lee).

http://dx.doi.org/10.1016/j.bbamem.2015.02.029
0005-2736/

$Asp^{2.50}$ results in the loss of function of receptor-G protein coupling [20–24]. The TM 2 domain is especially important for the stability of the seven TM domains to regulate its function and agonistic metal ion binding [16,25]. Despite its biological importance, the structure-function relationship of the Asp90 mutation is unknown.

A recent report demonstrated that sodium ions participate in allosteric modulation, bound to the highly conserved Asp residue in the TM 2 domain ($Asp^{2.50}$) [26], which serves as a heterozygous mutational site of MC4R. Here, we propose the structural properties of the TM 2 domain of MC4R, which are critical to its function. The solution structures of both $MC4R^{TM2}$ and the mutant are determined by circular dichroism (CD) and nuclear magnetic resonance (NMR) spectroscopy in a membrane environment. Moreover, data from analytical size-exclusion gel chromatography (aSEC) on MC4R and $MC4R^{D90N}$ strongly support the notion that the conformational transition of MC4R differs depending on the salt concentration, implying that Asp90 is a key residue that maintains the functional conformation of MC4R by sodium ion interaction.

2. Materials and methods

2.1. Cloning, purification, and NMR sample preparation of $MC4R^{TM2}$ and $MC4R^{TM2\text{-}D90N}$

A 5′-primer, including a DNA sequence-encoding thrombin cleavage site (LVPRGS) for removing the N-terminal His-tag from the target protein, and a 3′-primer, including a DNA sequence-encoding soluble KSI peptide (GGKKKK), were designed. DNA fragments encoding the highly conserved TM 2 domain of the melanocortin 4 receptor ($MC4R^{TM2}$) (Fig. 1A) were cloned into the plasmid pET21b (Promega) for co-expression with the hexa-histidine tag in the N-terminus. $MC4R^{TM2}$ was overexpressed in the *Escherichia coli* BL21 (DE3) strain (Novagen). Optical density in cell growth was measured up to 0.6 at 600 nm (OD600), and 1 mM isopropyl-1-thio-β-D-galactopyranoside (IPTG) was used as an inducer of protein overexpression. Cells were over-cultured for 15 h at 25 °C and harvested by centrifugation (6000 rpm, 30 min).

The cell pellets were dissolved in 20 mM Tris–HCl (pH 7.2), 200 mM NaCl, 5% glycerol (w/w), and 5 mM 2-mercaptoethanol and destroyed by sonication on ice. Then, the supernatant, including numerous soluble proteins, was separated from the cell broth by ultracentrifugation (17000 rpm, 30 min). The cell pellets were resuspended and solubilized in 20 mM Tris–HCl (pH 8.0), 200 mM NaCl, and 5 mM imidazole, including 6 M guanidine-HCl, for 5 h. After resolubilization, the soluble fraction was collected using ultracentrifugation (14000 rpm, 25 min). Recombinant proteins were purified using a Ni-NTA column (Amersham Biosciences), and the protein was eluted in 20 mM Tris–HCl (pH 8.0), 200 mM NaCl, and 350 mM imidazole, including 6 M guanidine-HCl, after column washing by 40 mM imidazole. The eluent was dialyzed in 1% acetonitrile and 0.01% trifluoroacetic acid (TFA) at room temperature for 12 h and lyophilized overnight. The white powder was dissolved in Tris–HCl (pH 7.6) and 200 mM urea and treated by thrombin enzyme (molar ratio = 1:15) for 4 h at 37 °C. The N-terminal His-tags were completely removed, and the final step of peptide purification was performed using a peptide-grade Superdex 75 Gel Filtration Column (Amersham Biosciences). The purity of the recombinant peptide was confirmed by MALDI-TOF Mass analysis. For the NMR experiments, $MC4R^{TM2}$ was labeled with $^{15}NH_4Cl$ and/or ^{13}C-labeled glucose in M9 media. $MC4R^{TM2\text{-}D90N}$ was generated by the quick mutagenesis

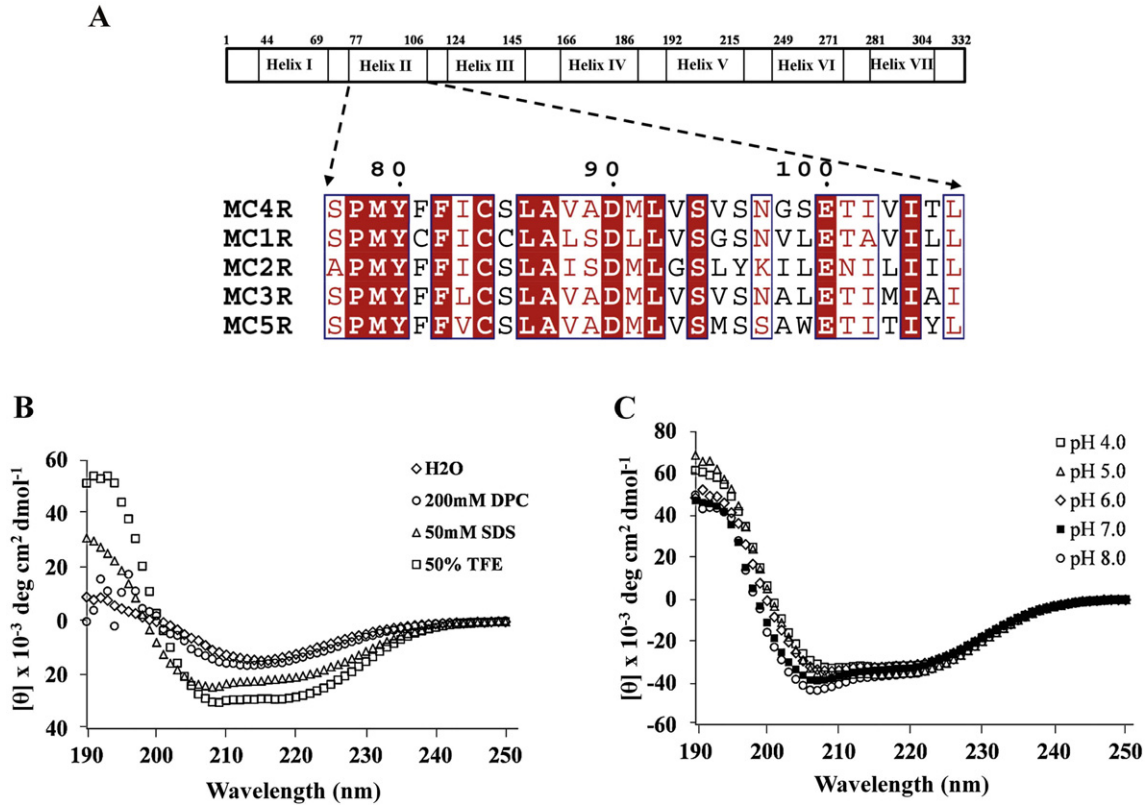

Fig. 1. Sequence alignment of MCRs and secondary structure analysis of $MC4R^{TM2}$ by CD spectroscopy. (A) Primary sequence alignment and schematic diagram of seven helix domains of MC4R were displayed. The MCRs are seven well-known TM GPCR families. All TM regions among them are conserved. Sequence alignment generated by ClustalW shows that the TM 2 domain is well conserved among the five human MCRs. The secondary structure of $MC4R^{TM2}$ was analyzed using CD (B) in different micelle conditions containing DPC, SDS, and TFE and (C) in different pH values from pH 4.0 to 8.0.

method, and the protein expression and purification processes were the same as those of $MC4R^{TM2}$.

2.2. Cloning, insect cell culture, and purification of MC4R and $MC4R^{D90N}$

The ΔN5-MC4R-T4L-ΔC10 (MC4R) and ΔN5-MC4R-D90N-T4L-ΔC10 ($MC4R^{D90N}$) receptor constructs were amplified using a codon-optimized synthetic gene (GenScript) as a template. The gene was inserted into the pFastBac-33A, which modified the pFastBac1 vector (Invitrogen) containing the hemagglutinin (HA) signal sequence (KTIIALSYIFCLVFA) at the N-terminus with a PreScission protease recognition sequence (LEVLFQG), a FLAG tag (DYKDDDDK), and a 10x His tag at the C-terminus, using AscI and FseI enzyme restriction sites. Generated constructs were transformed to the DH10Bac™ *E. coli* for transposition into the bacmid. Bacmid DNA was isolated using the ethanol precipitation method from inoculated white colonies. High-titer recombinant baculovirus stocks (>10^8 plaque forming units (pfu) per ml) were prepared using the Bac-to-Bac Baculovirus Expression System (Invitrogen). Next, 3ug of recombinant bacmid DNA containing the target gene were transfected into *Spodoptera frugiperda* (*Sf9*) cells (0.5×10^6 cells/ml) using 8ul of Lipofectamine®2000 Reagent (Life Technologies) and 100ul CCM3 media (HyClone™), and it was incubated for 3 days at 27 °C. The P1 virus stock was isolated by harvesting the supernatant after infection and used to generate the high-titer baculovirus stock. The *Sf9* cells (2×10^6 cells/ml) were infected by the P3 virus at an optimal MOI (multiplicity of infection, number of virus/number of cells) of 5 in Insectagro® media (Corning) and incubated at 27 °C. Target protein-expressed cells were harvested by centrifugation at 72 h post-infection and stored at −80 °C.

Frozen cell pellets were thawed in a hypotonic buffer containing 10 mM HEPES (pH 7.5), 10 mM $MgCl_2$, 20 mM KCl, and an EDTA-free protease inhibitor cocktail (Roche), and the isolated raw membrane was washed twice by dounce homogenization in the same hypotonic buffer. Thereafter, it was washed in a high osmotic buffer containing 10 mM HEPES (pH 7.5), 10 mM $MgCl_2$, 20 mM KCl, and 1.0 M NaCl three times. The purified membranes were resuspended in 10 mM HEPES (pH 7.5), 10 mM $MgCl_2$, 20 mM KCl, and 40% glycerol; flash-frozen in liquid nitrogen; and stored at −80 °C.

For the solubilization of MC4R, purified membranes were thawed on ice and preincubated with 500 μM antagonist SHU9119 (GenScript), 2.0 mg/ml iodoacetamide (Sigma), and an EDTA-free protease inhibitor cocktail (Roche). After preincubation for 20 min at 4 °C, membranes were solubilized in the presence of 800 mM NaCl, 0.5% (w/v) *n*-dodecyl-β-D-maltopyranoside (DDM) (Anatrace), and 0.1% (w/v) cholesteryl hemisuccinate (CHS) (Sigma) for 1.5 h at 4 °C. The solubilized fraction was isolated by ultracentrifugation at 150,000 × g for 40 min, and it was incubated with TALON IMAC resin (Clontech) overnight. Then, the resin was washed with 50 mM HEPES (pH 7.5), 800 mM NaCl, 10% (v/v) glycerol, 0.1% (w/v) DDM/0.02% (w/v) CHS, 10 mM $MgCl_2$, 8 mM ATP (Sigma), and 500 μM SHU9119 (GenScript). The second resin wash was done using 50 mM HEPES (pH 7.5), 150 mM NaCl, 10% (v/v) glycerol, 40 mM imidazole, 0.05% (w/v) DDM/0.01% (w/v) CHS, and 500 μM SHU9119. The MC4R was eluted with 50 mM HEPES (pH 7.5), 150 mM NaCl, 10% (v/v) glycerol, 250 mM imidazole, 0.05% (w/v) DDM/0.01% (w/v) CHS, and 500 μM SHU9119. The high-concentration imidazole was removed using a PD-10 Desalting Column (GE Healthcare) before the deglycosylation reaction. The PNGase enzyme was treated to target protein and mixture was incubated with TALON IMAC resin for 8 h. The second TALON resin work was performed, and the MC4R protein was eluted in 50 mM HEPES (pH 7.5), 150 mM NaCl, 10% (v/v) glycerol, 250 mM imidazole, 0.05% (w/v) DDM/0.01% (w/v) CHS, and 500 μM SHU9119. The purified MC4R in the presence of SHU9119 was concentrated from ~0.2 mg/ml to 30 mg/ml with a 100-kDa molecular weight cut-off Vivaspin Concentrator (GE Healthcare).

2.3. Analytical size-exclusion gel chromatography (aSEC)

The homogeneities of both MC4R and $MC4R^{D90N}$ proteins were confirmed for different NaCl concentrations from 0 mM to 500 mM. The ACQUITY UPLC System (Waters) and BEH Column (Waters) were used on 10 mM HEPES (pH 7.5), 10% glycerol, and 0.05% DDM/0.01% CHS with 0 mM, 75 mM, 150 mM, 300 mM, and 500 mM NaCl gradients. Six proteins, 400 kDa M.W. of Ferritin, 232 kDa M.W. of catalase, 158 kDa M.W. of aldolase, 43 kDa M.W. of ovalbumin, 20.4 kDa M.W. of chymotrypsin A and 13.7 kDa M.W. of Ribonuclease A was used for the standard curve fit for the size calculation.

2.4. Thermostability assay

Both MC4R and $MC4R^{D90N}$ proteins were purified in the presence of the antagonist SHU9119. N-[4-(7-diethylamino-4-methyl-3-coumarinyl) phenyl] maleimide (CPM) dye (Invitrogen) was dissolved in dimethyl sulfoxide (DMSO) (Sigma) at 4 mg/ml and stored at −80 °C. The CPM stock solution was then thawed and diluted 1:40 in dye dilution buffer (50 mM HEPES (pH 7.5), 150 mM NaCl, 10% glycerol, 0.05% DDM/0.01% CHS). The receptor (3 μg) was diluted in assay buffer (50 mM HEPES (pH 7.5), 150 mM NaCl, 10% glycerol, 0.05% DDM/0.01% CHS, 500 μM SHU9119) to a final volume of 200 μL, and the thermal denaturation assay was performed in a quartz fluorometer cuvette (Starna Cells, Inc., Atascadero, CA). All data were collected by a Cary Eclipse spectrofluorometer (Varian, USA) with a temperature ramping rate at 1 °C/min. The excitation wavelength was 387 nm, and the emission wavelength was 463 nm. All assays were performed over a temperature range of 20–95 °C.

2.5. CD spectroscopy

All CD spectra were recorded in 1 cm and 1 mm path length cylindrical cells for peptides in various conditions using a JASCO-J-810 spectropolarimeter. Eight consecutive scans were accumulated and averaged. The sample concentration was 50 μM, and micelle detergents were added to the peptide solution in 20 mM sodium phosphate (pH 7.0). CD spectra were detected with a 50 nm/min^{-1} scan speed, with a 190–250 nm UV range for different pH values. The population of the secondary structures was estimated using the K2d server (http://www.embl.de/~andrade/k2d/).

2.6. NMR spectroscopy and structure calculations

NMR experiments were performed using 2.5 mM $^{15}N/^{13}C$-labeled $MC4R^{TM2}$ and $MC4R^{TM2\text{-}D90N}$. Lyophilized protein sample was dissolved in 20 mM sodium phosphate (pH 7.0), 40 mM DTT, 0.01% sodium azide, 200 mM deuterium-labeled SDS, and 10% D_2O. NMR experiments were performed on Bruker DRX-500 and DRX-600 spectrometers in quadrature detection mode using a triple-resonance probe equipped with an actively shielded pulsed field gradient (PFG) coil. All NMR data were collected at 303 K. Data were processed using NMRPipe/NMRDraw [27] or XWIN-NMR (Bruker Instruments) software on a Silicon Graphics Indigo^2 workstation and analyzed using the Sparky 3.113 program [28]. Sequential resonance assignment was executed by ^1H–^{15}N heteronuclear single quantum coherence [29] and three-dimensional (3D) HNCACB, CBCACON and HBHACONH, HCCH-total correlation spectroscopy (TOCSY) experiments [29–35]. Together with the assigned resonance chemical shift values and peak intensity values obtained in 3D ^{15}N-edited nuclear overhauser effect spectroscopy (NOESY) (m = 150 ms) [36] and ^{13}C-edited NOESY (m = 150 ms) HSQC [37] spectra, the structure calculation was

performed using the CYANA program version 2.2.5 [38] on a Linux cluster with 16 nodes. The phi and psi values obtained by the TALOS program [39] were added during the CYANA program process as a structural restraint. Sequential nuclear overhauser effects (NOEs) and typical α-helix NOEs were detected in the NOESY spectra and were well matched with the TALOS result. Around Gln97, Gly98, and Ser99, not enough NOEs were detected due to dynamics nature and the kink region of the MC4R^{TM2}. Hydrogen bonds were determined from the preliminary structures and amide proton exchange experiment. A total of 233 unambiguous NOEs and 19 hydrogen bonds were used for structure calculations. The final refined structures were analyzed and visualized with PROCHECK [40], PyMOL [41], and MOLMOL [42]. Refinement of solution structure of MC4R^{TM2} was done by molecular dynamics simulations as previously reported [43,44].

2.7. Molecular modeling

An atomic-resolution structure of MC4R was constructed using the homology modeling method. The procedures of homology modeling, which are optimized for GPCRs, can be divided into five steps: template selection, alignment, model building, helix optimization, and loop optimization. First, amino acid sequences of human MC4R were obtained from the NCBI database (http://www.ncbi.nlm.nih.gov/), and a basic local alignment search tool (BLAST) search was performed in the protein data bank (PDB) database to select the template. The B2 adrenergic receptor (B2AR, PDB ID: 2RH1) showed the nineteen percent of sequence identities with MC4R in the BLAST results, so we chose B2AR as the template and performed manual sequence alignment between B2AR and MC4R on the basis of the positions of GPCR conserved motifs in each TM. Subsequently, the constructed helix and loop parts of MC4R were separated based on the template. Seven helices were built using the template-structure-based approach with the Prime [45] homology modeling tool of Schrödinger suites, and six extra- and intra-cellular loops were created using the *de novo* loop creation tool in BioLuminate [46], also of Schrödinger suites. The helix and loop parts were built separately, as GPCR loop structures are as diverse in their lengths, shapes, and amino acid compositions as the species, whereas helix structures are rather constant across different species. As a result, there is no robust template to use for loop-structure building, and thus, the loop structures were built using the energy-based approach. Optimizations were also processed separately. First, we refined the side-chain conformations of helix regions using Prime's side-chain refinement tool. In this step, the implicit membrane was imposed on the helix regions for the precise refinement of the exterior side chains. Next, we performed simulated annealing dynamics to find the globally optimized conformation of the loops using Desmond [47]. The simulation was run for 20 ns at 100–400 K, and the POPC (1-palmitoyl-2-oleoyl-sn-glycero-3-phosphocholine) explicit membrane was assumed in the helix regions, which were fixed by force constraints. Before the simulation, we put a sodium atom similar to that of the A2A adenosine receptor crystal structure [48] in the sodium allosteric binding site and placed water molecules around it.

3. Results

3.1. Expression and purification of MC4R^{TM2}

MC4R^{TM2} was identified by BLAST search and sequence alignment. The primary sequence alignment showed that the TM 2 domain of MC4R was well conserved among human MCR families (Fig. 1A). MC4R^{TM2} and MC4R$^{TM2\text{-}D90N}$ were successfully inserted in the pET21b vector, and it was expressed in the *E. coli* system. To obtain uniformly ^{13}C- and ^{15}N-labeled MC4R^{TM2} and MC4R$^{TM2\text{-}D90N}$ for structural studies, M9 minimal media was used for bacterial culture. The final peptide yield was approximately 15 mg according to 500 ml cell culture, and peptide purity was over 90% according to MALDI-TOF Mass analysis.

3.2. Structural analysis by CD spectroscopy

CD spectra were acquired on MC4R^{TM2} under DPC, SDS micelle, TFE and different pH conditions. To determine optimal micelle conditions, all CD spectra were measured in the same peptide concentration of 50 μM in 20 mM sodium phosphate (pH 7.0) but with different micelle detergents. Data showed that MC4R^{TM2} contained a low helical content of about 28% and 39% in H_2O and 200 mM dodecylphosphocholine (DPC) micelle conditions, respectively. However, the characteristic α-helical populations were observed for MC4R^{TM2} in both 50 mM SDS and 50% tetrafluoroethylene (TFE) solution (Fig. 1B): a typical double minima of transition (n-π*) at 208 and 222 nm and a maximum of transition (π-π*) at 192 nm. Around eighty-four percent of helical contents were observe in both the 50 mM SDS and 50% TFE conditions (Fig. 1B). However, there were no significant structural changes for different pH values (Fig. 1C). Data from the CD spectrum suggest that MC4R^{TM2} forms an α-helical structure in the presence of an SDS micelle environment.

3.3. NMR resonance assignments

A series of ^{1}H–^{15}N 2D HSQC spectra were collected for different detergent conditions (TFE, DPC, SDS) (data was not shown). MC4R^{TM2} showed the maximum helical population and homogeneity at the 200 mM SDS micelle condition. The NMR experimental condition was optimized by a series of ^{1}H–^{15}N 2D HSQC spectra for different pH conditions. The NMR spectra at 200 mM SDS and pH 7.0 showed that most of the NH/C$^{\alpha}$H resonances were well separated, indicating homogeneity of the MC4R^{TM2} conformation (Fig. 2A).

Both backbone and side-chain assignments were done by following the correlation of the NH group to the preceding Cα and Cβ chemical shifts, and the side-chain proton resonances were easily identified by HCCH-TOCSY connectivity (Fig. 2A). Backbone assignment was completely assigned and 90% of carbon and 95% of proton of sidechain atom were assigned. The secondary structures of MC4R^{TM2} were confirmed by following $d_{\alpha N}$ (i, i + 1), d_{NN} (i, i + 1) NOE connectivities in the NOESY spectrum [49] (Fig. 2B) with both the TALOS and CSI (chemical shift index) programs. NMR data suggested that MC4R^{TM2} forms a long α-helix with a kink at Gly98. The long α-helix is composed of two regions from Met79 to Asn97 and Gln100 to Thr105 (Fig. 2B).

3.4. Solution NMR structure of MC4R^{TM2}

The 20 energy-minimized NMR structures of MC4R^{TM2} were calculated from the 100 initial structures. The average target function value was 0.251 ± 0.0181. No violations for distance constraints were detected during structure calculation. The mean root mean square deviation (RMSD) values of backbone atoms and all heavy atoms from Tyr80 to Asn97 were 0.671 ± 0.05 and 0.793 ± 0.03, respectively (Fig. 3A). In addition, the mean RMSD values of backbone atoms and all heavy atoms from Thr101 to Leu106 were 0.566 ± 0.03 and 0.623 ± 0.01, respectively (Fig. 3B). The phi–psi dihedral angles of the final structures were appropriately distributed in the Ramachandran plot. The values were 86.8%, and 13.2%, in most favored and additionally allowed regions, respectively. After the structural refinement via molecular dynamics simulation methods, overall structure of MC4R^{TM2} was stabilized after 1 ns and average RMSD of heave atoms was 2.3566. The ribbon drawing of the MC4R^{TM2} structure with all side-chain atoms provides a clear picture of the kink at the end of the helix (Fig. 3C). Structure statistics and structure quality factors are shown in Table 1. Helix bending in the TM2 of the GPCRs is observed and it may allow the structural diversity within the GPCR family [50]. To understand common structural properties of TM2 in GPCRs, we superimposed solution structure of

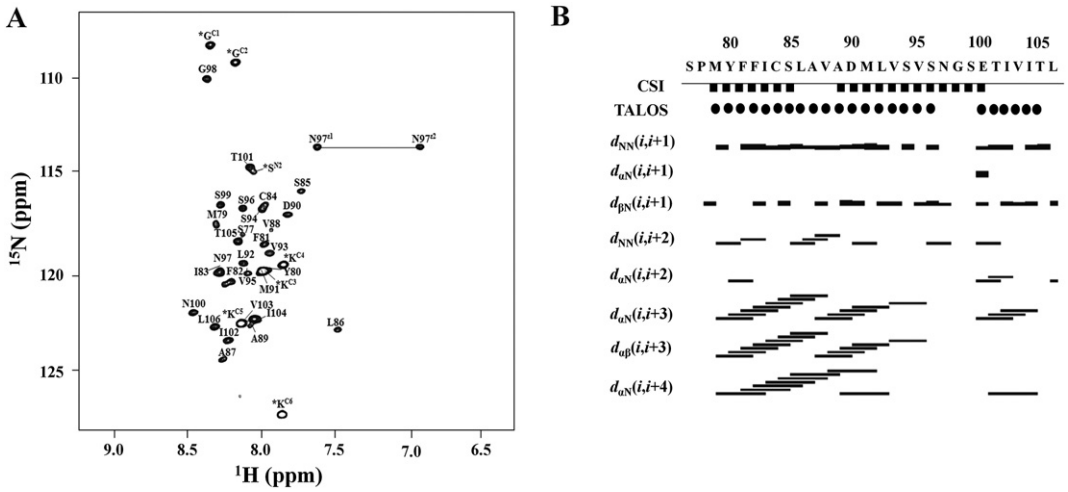

Fig. 2. Backbone assignment and NOE bar diagram of MC4R^{TM2}. (A) ^{1}H–^{15}N HSQC spectra of MC4R^{TM2} were collected in 20 mM sodium phosphate (pH 7.0), 40 mM DTT, 0.01% sodium azide, 200 mM deuterium-labeled SDS, and 10% D_2O at 303 K. All resonances were assigned using triple resonance NMR data. Asterisks (*) indicate extra residues from the KSI tag ($G^{C1}GKKKK^{C6}$). (B) A summary of NOEs indicates the α-helical structure of MC4R^{TM2}. The thickness of NOEs shows the NOE cross-peak intensity. The secondary structure of MC4R^{TM2} was confirmed by the CSI (filled squares) and TALOS (filled circles) programs using experimental data.

MC4R^{TM2} with that of crystal structures of A2A adenosine receptor and B2 adrenergic receptor (Fig. 3D).

3.5. Structural comparison between MC4R^{TM2} and MC4R$^{TM2\text{-}D90N}$

To observe the structural difference between MC4R^{TM2} and MC4R$^{TM2\text{-}D90N}$, the MC4R$^{TM2\text{-}D90N}$ peptide was prepared in the same way as MC4R^{TM2}. The backbone resonance assignments of MC4R$^{TM2\text{-}D90N}$ were completed using data from HNCACB and HNCA (Fig. 4A). The amide-proton chemical shift of MC4R$^{TM2\text{-}D90N}$ was very similar to and overlapped well with that of MC4R^{TM2}. The substitution from Asp90 to Asn90 was directly confirmed by the backbone resonance assignments (Fig. 4A). Using the Cα and Cβ chemical shift values, the phi–psi dihedral angles were calculated with the TALOS program. The secondary structure of MC4R$^{TM2\text{-}D90N}$ predicted by CSI was the same as that of MC4R^{TM2} (Fig. 4B). Similarly, data from CD confirmed that MC4R$^{TM2\text{-}D90N}$ forms an α-helix in SDS micelle conditions (Fig. 4C).

3.6. Thermal stability and homogeneity of MC4R and MC4R^{D90N}

The thermal stability and homogeneity of MC4R and MC4R^{D90N} were measured by aSEC and CPM fluorescence spectroscopy assay in 50 mM HEPES (pH 7.5), 150 mM NaCl, 0.05% DDM/0.01% CHS, 10% glycerol, and 500 μM SHU9119. Data from aSEC showed that structural homogeneity was changed by point mutation at Asp90. MC4R^{D90N} was less stable than MC4R (Fig. 5A). The CPM fluorescence spectroscopy based on the binding of the thiol-specific maleimide CPM to cysteines showed that the melting curves of both MC4R and MC4R^{D90N} had clear transitions at 60 °C and 56 °C, respectively (Fig. 5B). The thermal stability result indicated that mutation led MC4R^{D90N} to become unstable.

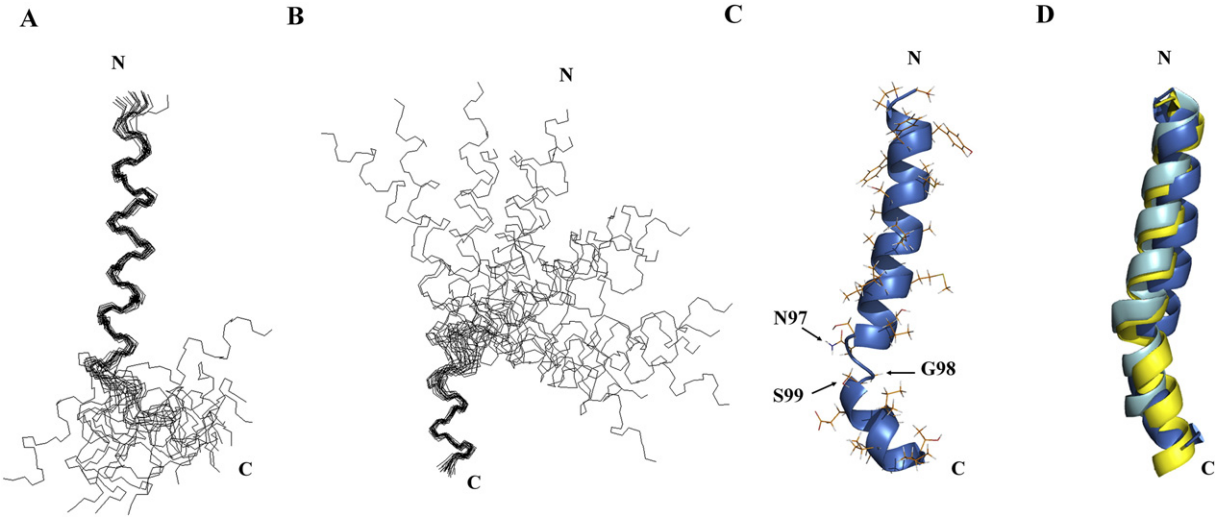

Fig. 3. Solution structures of MC4R^{TM2}. The 20 structures of MC4R^{TM2} over the energy-minimized average structure (generated by MOLMOL) are superimposed for (A) Met 79-Asn97 and (B) Asn97-Leu106 in stereoview, respectively. (C) The average structure of MC4R^{TM2} is represented by a ribbon diagram, and the side chains are colored in yellow. Three residues located in the structural dynamics region between two helices are indicated by an arrow. The image was generated by PyMOL. (D) The Structural superimposition of TM2 region among three GPCR receptors based on sequence alignment have shown similar kink shape in TM2, although the patterns and degree of kink region are different. The TM2 from MC4R, A2A adenosine receptor and B2 adrenergic receptor are colored by blue, cyan and yellow, respectively.

Table 1
Structural statistics and mean squared deviations (RMSD) for the 20 lowest-energy structure of MC4R TM2$^{77-106}$.

Experiment distance constraints	MC4R TM2$^{77-106}$
NOE distance constraints	
Total	233
Sequential, |i–j| = 1	87
Short-range, |i–j| ≤ 1	161
Medium range, 1 < |i–j| < 5	72
Intra-residue, |i–j| = 0	74
Hydrogen bond constraints	19
Dihedral constraints	
All	17
Φ	8
Ψ	9
Mean CYANA target function (Å^2)	0.231 ± 0.028
Number of restraint violations	
Total number of distance violations >0.5 Å	0
Total number of hydrogen bond violation >0.5 Å	0
Total number of dihedral angle violations >5	0
Mean RMS deviations from the average coordinate (Å)[a]	
Backbone atoms of residues (80–97)	0.671 ± 0.05
Heavy atoms (80–97)	0.793 ± 0.03
Backbone atoms of residues (101–106)	0.566 ± 0.03
Heavy atoms (101–106)	0.623 ± 0.01
Ramachandran plot (%)[a]	
Residues in most favored regions	86.8
Residues in additional allowed regions	13.2
Residues in generously allowed regions	0.0
Residues in disallowed regions	0.0

[a] Ramachandran plot was calculated using the PROCHECK program.

3.7. Salt effect on MC4R and MC4R^{D90N}

To understand the effect of sodium ion on MC4R and MC4R^{D90N}, we performed aSEC in different salt concentration (0 mM–500 mM). While uniform conformational states of MC4R were observed for different salt concentrations (Fig. 6A), inhomogeneous states were detected for MC4R^{D90N} (Fig. 6B). According to column calibration, retention time of 5.6 min demonstrates dimeric size of MC4R (119.4 kDa) while 5.9 min is the monomeric size (62 kDa). Since GPCR function is related to not only conformational change but oligomerization status, we investigated the structural integrity of both MC4R and MC4R^{D90N} for different salt concentrations. Our data suggests that salt concentration plays a role for oligomerization process of MC4R. MC4R^{D90N} fails salt-mediated oligomerization process, resulting loss of its function. Therefore, we concluded that Asp90$^{2.50}$ residue plays an important role in both the stability and homogeneity of MC4R upon sodium binding.

3.8. Sodium ion binding site of MC4R

In general, seven TMs in GPCR structure have extensive hydrogen bond network and they interact with water and sodium ion in direct or indirect manner. Recent studies have shown that the interaction between water and sodium ion is important for GPCR function. Our data suggest that the hydrogen bond network and sodium ion interaction are highly related in GPCR function. Data from the temperature coefficients of the amide protons of MC4R^{TM2} represented that both Leu86 and Asp90 showed relatively high temperature coefficients in the sodium-binding pocket (Fig. 6C). Therefore, we propose the structural clue for the sodium ion binding during conformational modulation of MC4R [51,52]. The modeling structure of MC4R in the presence of sodium ions based on the crystal structure of B2AR demonstrated that both sodium ions and water molecules were co-oriented to conserve the allosteric pocket (Fig. 7A). The modeling structure of MC4R suggested that sodium ions coordinated the conserved residues of MC4R in the allosteric sodium-binding pocket together with several water molecules. The distance between sodium ion and water molecules was measured as 2–3 Å. Asp90$^{2.50}$, Ser136$^{3.39}$, and Asp294$^{7.49}$ residues largely participated in sodium ion binding (Fig. 7B). The superimposed structures of A2AAR, B2AR, and CXCR4 with MC4R support this hypothesis, showing that the residues in the allosteric sodium ion binding pocket of Class A GPCRs were well conserved (Fig. 7C and D).

4. Discussion

In this study, we presented the structural role of Asp90$^{2.50}$ of MC4R as a key residue in the sodium ion allosteric pocket. Recent GPCR studies suggest that the Asp$^{2.50}$ residue in the TM 2 domain of GPCRs is involved in structural and functional diverse by interaction with the NPxxY motif.

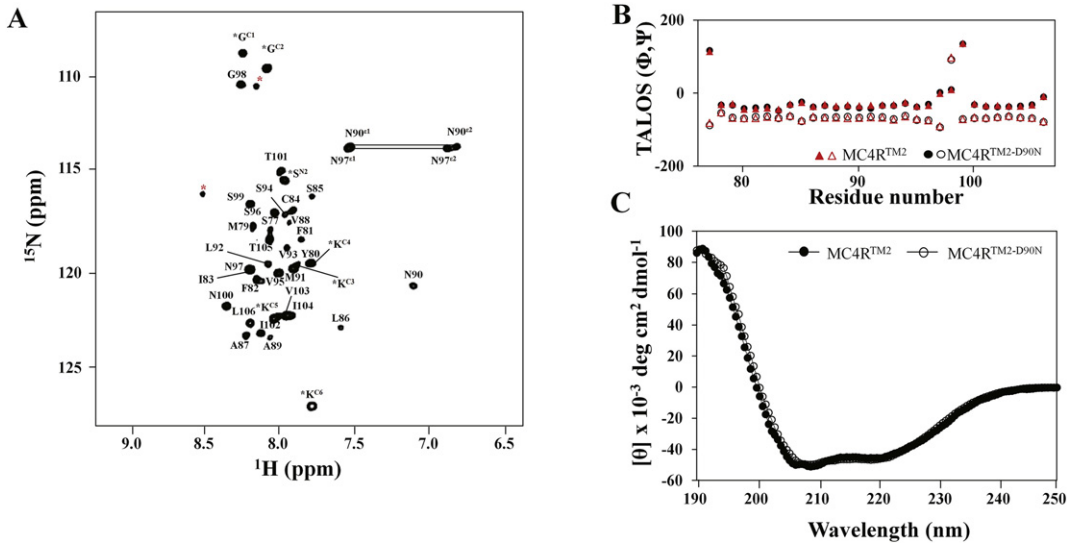

Fig. 4. Backbone assignment and secondary structures of MC4R$^{TM2-D90N}$. (A) ^{1}H–^{15}N HSQC spectra of MC4R$^{TM2-D90N}$ were collected in 20 mM sodium phosphate (pH 7.0), 40 mM DTT, 0.01% sodium azide, 200 mM deuterium-labeled SDS, and 10% D_2O at 303 K. All peaks were completely assigned using backbone datasets. Asterisks (*) indicate extra residues from the KSI tag (G^{C1}GKKKK^{C6}). (B) Phi and psi torsion angles of MC4R$^{TM2-D90N}$ (Φ — open circle and Ψ — filled circle colored in black) obtained from the TALOS program are compared with that of MC4R^{TM2} (Φ — open triangle and Ψ — filled triangle colored in red). The psi and phi angle values suggest that both MC4R^{TM2} and MC4R$^{TM2-D90N}$ have α-helical structures in SDS micelles. (C) The secondary structures of both MC4R^{TM2} (filled circle) and MC4R$^{TM2-D90N}$ (open circle) were analyzed using CD spectroscopy in 20 mM sodium phosphate (pH 7.0), 50 mM SDS.

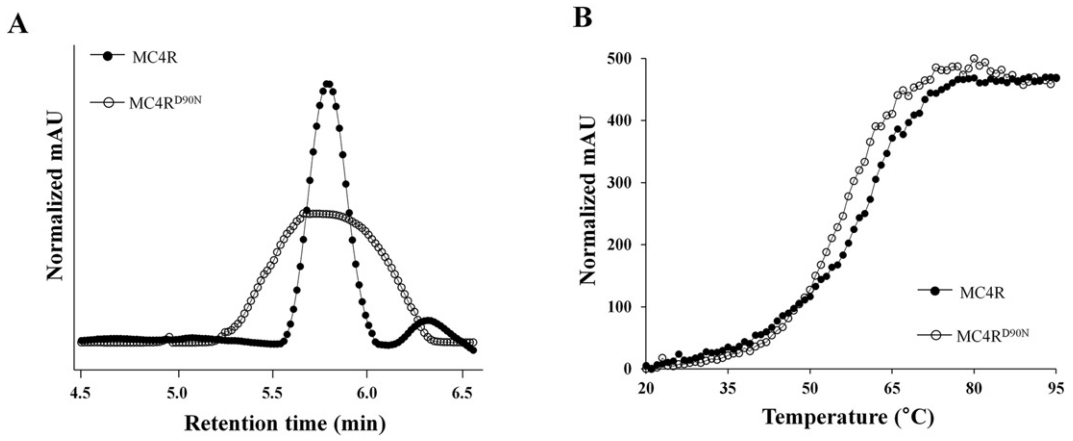

Fig. 5. Measurement of conformational homogeneity and thermal stability of MC4R and MC4R^{D90N}. (A) The conformational homogeneity of MC4R (filled circle) and MC4R^{D90N} (empty circle) was measured by aSEC traces. (B) The thermal stability of MC4R (filled circle) and MC4R^{D90N} (empty circle) was measured. Melting temperatures (T_m) were determined by fitting the curves to a Boltzmann sigmoidal equation and were as follows: MC4R, $T_m = 60$ °C; MC4R^{D90N}, $T_m = 56$ °C.

In the same manner, the Asn$^{7.49}$ residue in the NPxxY motif is also involved in the sodium ion allosteric pocket and plays the role of a switch for both the active and inactive conformation of GPCRs [53,54]. In addition, recent papers proposed that when distances between Asn322$^{7.49}$ in the NPxxY motif and Asp79$^{2.50}$ of B2AR in the agonist, inverse agonist, and Apo states were measured, the distance between Asn322$^{7.49}$ and Asp79$^{2.50}$ was small in the active state. In contrast, the distance between Asn322$^{7.49}$ and Asp79$^{2.50}$ was large in the inactive state by the side-chain orientation of Asn322$^{7.49}$, indicating that the inter-helical space becomes wider to provide enough space for sodium ion interaction [26,55].

However, although MC4R has a conserved sodium ion allosteric pocket similar to other Class A GPCR family proteins, Asp90$^{2.50}$ interacts with Asn294$^{7.49}$, which is not located in the NPxxY motif. Because of the conserved motif of the NPxxY substitute to DPxxY in MC4R, the signaling mechanism of MC4R would differ from that of other Class A GPCR family proteins. For example, the opsin receptor in the active state has a hydrogen-bond interaction between Asn302$^{7.49}$ and Tyr306 in the

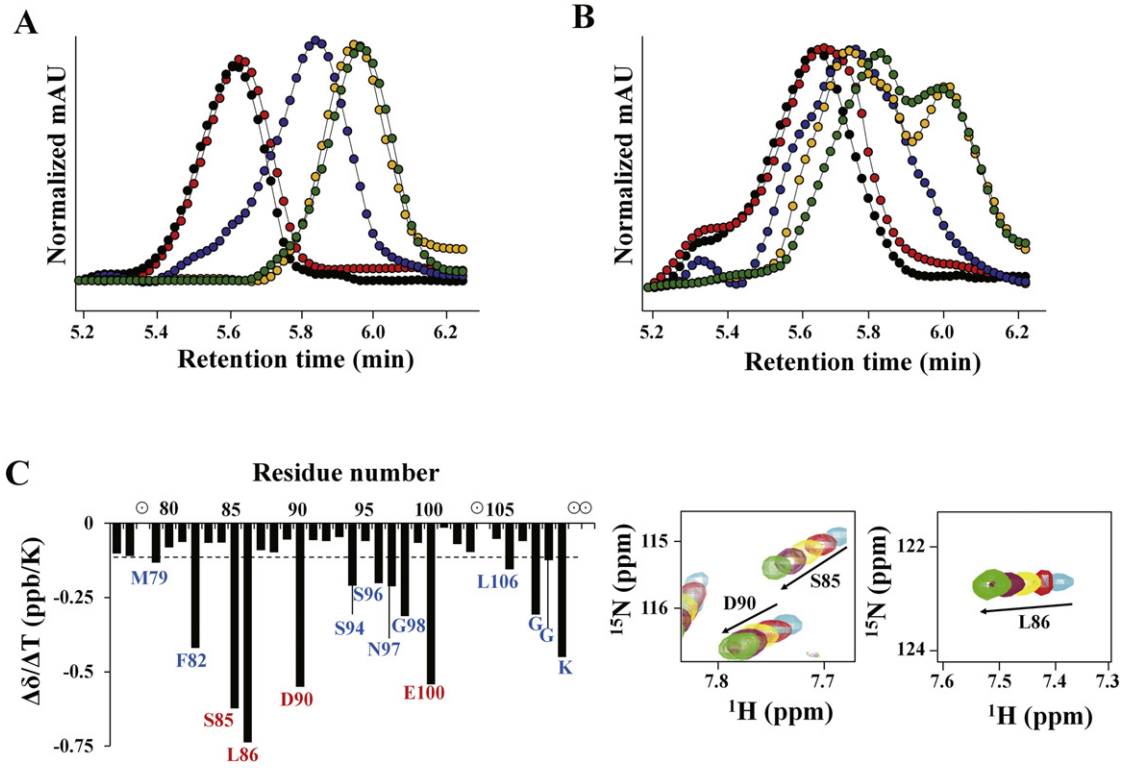

Fig. 6. Salt effect on MC4R and MC4R^{D90N} and temperature coefficient experiment for MC4R^{TM2}. (A) aSEC traces of MC4R with five different salt conditions (0 mM (colored in black), 75 mM (colored in red), 150 mM (colored in blue), 300 mM (colored in yellow), and 500 mM (colored in green)) were represented. Retention time was shifted by increasing salt concentration. (B) aSEC traces of MC4R^{D90N} with five different salt conditions (0 mM (colored in black), 75 mM (colored in red), 150 mM (colored in blue), 300 mM (colored in yellow), and 500 mM (colored in green)) were shown. Retention time was shifted by increasing salt concentration. (C) Temperature coefficients ($\Delta\delta/\Delta T$) of amide protons of MC4R^{TM2} were measured in 20 mM sodium phosphate (pH 7.0), 40 mM DTT, 0.01% sodium azide, 200 mM deuterium-labeled SDS, and 10% D_2O at five different temperatures. The temperature coefficients were obtained by linear fitting of the amide chemical shift (δ_{HN}) as a function of temperature measured at 25 °C (cyan), 30 °C (red), 35 °C (yellow), 40 °C (magenta), and 45 °C (green). One residue is proline and, the others, because of poor signal sensitivity of signal to noise, we could not confirmed those peaks during temperature coefficient test. The undetected peaks are labeled as ⊙.

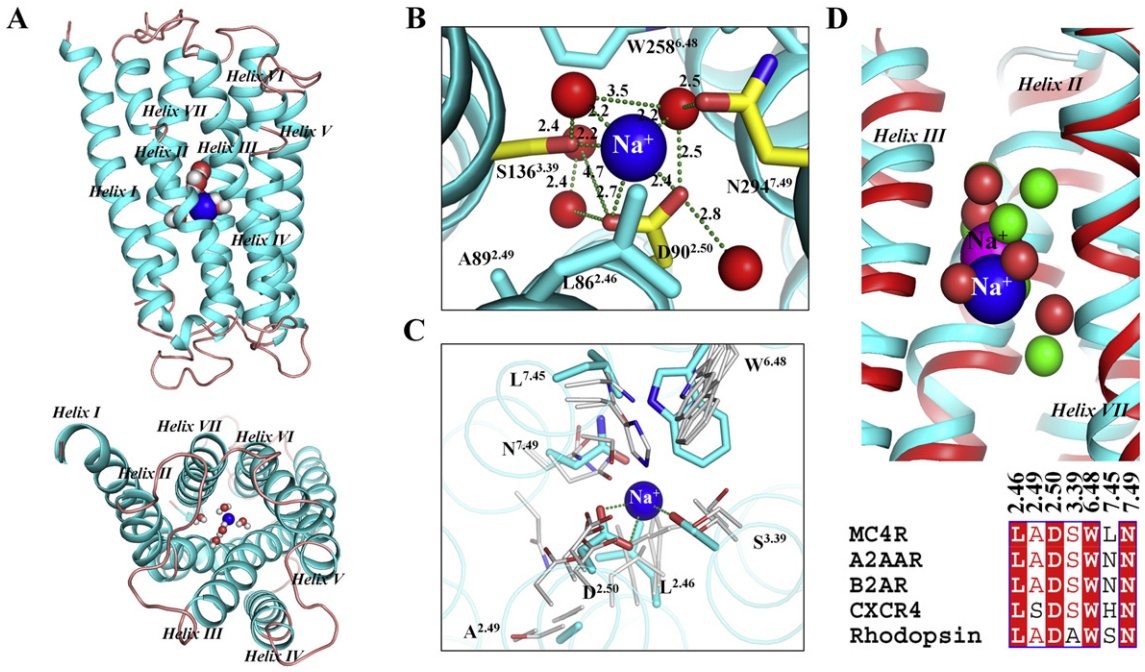

Fig. 7. Modeling structure of MC4R and structural insight of conserved sodium ion allosteric pocket. (A) A 3D structure of MC4R with sodium ions was generated by homology modeling. (B) Allosteric sodium ion binding pocket of MC4R with water molecules (red sphere) and sodium ions (blue sphere) were displayed. Water molecules surround sodium ions, stabilizing Helices 2, 3, and 7. (C) Side-chain orientations of residues in sodium ion allosteric pocket of MC4R were looked in detail. Asn90 is a key residue for sodium ion interaction. (D) Structural comparison between MC4R and A2AAR displays intermolecular interaction between sodium ions (blue and violet sphere for MC4R and A2AAR) and water molecules (red and green sphere for MC4R and A2AAR).

NPxxY motif. This interaction is broken in the hMC4R model, and Asp298 (DPxxY) interacts with Asn294$^{7.49}$ instead [56]. The mutational study of 5-HT$_{2A}$, including the NPxxY and DPxxY motifs, already proves that the molecular selectivity with interacting proteins, such as ARF1 and ARF6, was shifted in Asn (N)/Asp (D) substitution [57]. Furthermore, in many cases of other GPCRs, it has been proposed that sodium ions bind in an allosteric site (Asp$^{2.50}$) located in the TM 2 domain and act as allosteric modulators [58–60]. The high-resolution X-ray crystal structure of A2AAR coordinated with the sodium ion and conserved water molecules in the center of the seven TM bundles clearly supports the vital role of sodium ions in GPCR functions [48]. Therefore, Asp90$^{2.50}$ located in the sodium ion allosteric binding pocket plays a key role in not only mediating allosteric regulation by sodium ion interaction but also enabling the switch between active and inactive conformation through NPxxY motif interaction.

In our study, the NMR structure of MC4R^{TM2} revealed an α-helix conformation with a kink similar to that of solved GPCR structures. The helical bend in the TM 2 domain is not unusual, and it is partially responsible for multilithic TM functions [24]. Interestingly, we found that the temperature coefficients of four residues such as Ser85, Leu86, Asp90, and Glu100 were relatively large, as shown in Fig. 6C. This is also explainable in terms of the dynamic nature of the TM 2 domain. Data from NMR and CD spectroscopy show that the secondary structure of MC4R$^{TM2\text{-}D90N}$ is not affected by substitution from Asp90 to Asn90. However, the stability and homogeneity of MC4R are dramatically changed upon point mutation due to the different interaction modes with sodium ions and the DPxxY motif. Our data strongly suggest a dominant negative effect of the heterozygous MC4R mutant. In addition, although MC4R has a tendency to maintain a single conformation for different sodium ion concentrations, MC4R^{D90N} does not have a stable conformation, meaning that the mutant protein cannot form either the active or the inactive saturated state. Our results suggest that MC4R is necessary to ensure the optimum efficacy of sodium ions and maintain the stable dimer or oligomer formation of MC4R in a function and that the TM 2 domain plays a role as the pivot of conformational switch of MC4R.

Conflict of interest statement

The authors declare that the research was conducted in the absence of any commercial or financial relationships that could be construed as a potential conflict of interest.

Acknowledgements

We would like to thank Kurt Wüthrich for fruitful discussions on this research. This work was supported by Mid-career Researcher Program (NRF-2013R1A2A2A01068963) through NRF grant funded by the MEST. AEC and MSK were supported by NRF Grants No. 2012R1A1A2043211, 2013R1A2A2A01067638, and 2012M3C1A6035362. J.H. Yun is a recipient of Brain Korea Plus (BK+) grant.

References

[1] K.G. Mountjoy, L.S. Robbins, M.T. Mortrud, R.D. Cone, The cloning of a family of genes that encode the melanocortin receptors, Science 257 (1992) 1248–1251.
[2] A.S. Chen, D.J. Marsh, M.E. Trumbauer, E.G. Frazier, X.M. Guan, H. Yu, C.I. Rosenblum, A. Vongs, Y. Feng, L. Cao, J.M. Metzger, A.M. Strack, R.E. Camacho, T.N. Mellin, C.N. Nunes, W. Min, J. Fisher, S. Gopal-Truter, D.E. Maclntyre, H.Y. Chen, L.H. Van der Ploeg, Inactivation of the mouse melanocortin-3 receptor results in increased fat mass and reduced lean body mass, Nat. Genet. 26 (2000) 97–102.
[3] A.A. Butler, R.A. Kesterson, K. Khong, M.J. Cullen, M.A. Pelleymounter, J. Dekoning, M. Baetscher, R.D. Cone, A unique metabolic syndrome causes obesity in the melanocortin-3 receptor-deficient mouse, Endocrinology 141 (2000) 3518–3521.
[4] W. Fan, B.A. Boston, R.A. Kesterson, V.J. Hruby, R.D. Cone, Role of melanocortinergic neurons in feeding and the agouti obesity syndrome, Nature 385 (1997) 165–168.
[5] D. Huszar, C.A. Dynch, V. Fairchild-Huntress, J.H. Dunmore, Q. Fang, L.R. Berkemeier, W. Gu, R.A. Kesterson, B.A. Boton, R.D. Cone, F.J. Smith, L.A. Campfield, P. Burn, F. Lee, Targeted disruption of the melanocortin-4 receptor results in obesity in mice, Cell 88 (1997) 131–141.

[6] H. Wessells, V.J. Hruby, J. Hackett, G. Han, P. Balse-Srinivasan, T.W. Vanderah, Ac-Nle-c[Asp-His-DPhe-Arg-Trp-Lys]-NH2 induces penile erection via brain and spinal melanocortin receptors, Neuroscience 118 (2003) 755–762.
[7] L. Fani, S. Bak, P. Delhanty, E.F. van Rossum, E.L. van den Akker, The melanocortin-4 receptor as target for obesity treatment: a systematic review of emerging pharmacological therapeutic options, Int. J. Obes. 38 (2014) 163–169.
[8] I. Gantz, H. Miwa, Y. Konda, Y. Shimoto, T. Tashiro, S.J. Watson, J. Delvalle, T. Yamada, Molecular cloning, expression, and gene localization of a fourth melanocortin receptor, J. Biol. Chem. 268 (1993) 15174–15179.
[9] K.S. Graham, R.L. Leibel, Yellow mice, red hair, and childhood obesity: the melanocortinergic pathway in energy homeostasis, J. Pediatr. 139 (2001) 177–181.
[10] H. Biebermann, H. Krude, A. Elsne, V. Chubanov, T. Gudermann, A. Grüters, Autosomal-dominant mode of inheritance of a melanocortin-4 receptor mutation in a patient with severe early-onset obesity is due to a dominant-negative effect caused by receptor dimerization, Diabetes 52 (2003) 2984–2988.
[11] R.D. Cone, The central melanocortin system and energy homeostasis, Trends Endocrinol. Metab. 10 (1999) 211–261.
[12] C. Vaisse, K. Clément, E. Durand, S. Hercberg, B. Guy-Grand, P. Froguel, Melanocortin-4 receptor mutations are a frequent and heterogeneous cause of morbid obesity, J. Clin. Invest. 106 (2000) 253–262.
[13] I.S. Farooqi, G.S.H. Yeo, J.M. Keogh, S. Aminian, S.A. Jebb, G. Butler, T. Cheetham, S. O'Rahilly, Dominant and recessive inheritance of morbid obesity associated with melanocortin 4 receptor deficiency, J. Clin. Invest. 106 (2000) 271–279.
[14] H. Kobayashi, Y. Ogawa, M. Shintani, K. Ebihara, M. Shimodahira, T. Iwakura, M. Hino, T. Ishihara, K. Ikekubo, H. Kurahachi, K. Nakao, A novel homozygous missense mutation of melanocortin-4 receptor (MC4R) in a Japanese woman with severe obesity, Diabetes 51 (2002) 243–246.
[15] P.J. Delhanty, E. Bouw, M. Huisman, R.M. Vervenne, A.P. Themmen, A.J. van der Lely, E.L. van den Akker, Functional characterization of a new human melanocortin-4 receptor homozygous mutation (N72K) that is associated with early-onset obesity, Mol. Biol. Rep. 1007 (2014) (11033-014-3691-7).
[16] C. Govaerts, S. Srinivasan, A. Shapiro, S. Zhang, F. Picard, K. Clement, C. Lubrano-Berthelier, C. Vaisse, Obesity-associated mutations in the melanocortin 4 receptor provide novel insights into its function, Peptides 26 (2005) 1909–1919.
[17] C. Lubrano-Berthelier, E. Durand, B. Dubern, A. Shapiro, P. Dazin, J. Weill, C. Ferron, P. Froguel, C. Vaisse, Intracellular retention is a common characteristic of childhood obesity-associated MC4R mutations, Hum. Mol. Genet. 12 (2003) 145–153.
[18] Y.X. Tao, Molecular mechanisms of the neural melanocortin receptor dysfunction in severe early onset obesity, Mol. Cell. Endocrinol. 239 (2005) 1–14.
[19] J.A. Ballesteros, L. Shi, J.A. Javitch, Structural mimicry in G protein-coupled receptors: implications of the high-resolution structure of rhodopsin for structure–function analysis of rhodopsin-like receptors, Mol. Pharmacol. 60 (2001) 1–19.
[20] B.P. Ceresa, L.E. Limbird, Mutation of an aspartate residue highly conserved among G-protein-coupled receptors results in nonreciprocal disruption of α2-adrenergic receptor-G-protein interaction, J. Biol. Chem. 269 (1994) 29557–29564.
[21] J.P. Roche, S. Bounds, S. Brown, L. Mackie, A mutation in the second transmembrane region of the CB1 receptor selectively disrupts G protein signaling and prevents receptor internalization, Mol. Pharmacol. 56 (1999) 611–618.
[22] Q. Tao, M.E. Abood, Mutation of a highly conserved aspartate residue in the second transmembrane domain of the cannabinoid receptors, CB1 and CB2, disrupts G-protein coupling, J. Pharmacol. Exp. Ther. 295 (1998) 651–658.
[23] P.P. Lakhlani, L.B. MacMillan, T.Z. Guo, B.A. McCool, D.M. Lovinger, M. Maze, L.E. Limbird, Substitution of a mutant alpha2a-adrenergic receptor via "hit and run" gene targeting reveals the role of this subtype in sedative, analgesic, and anesthetic-sparing responses in vivo, Proc. Natl. Acad. Sci. 94 (1997) 9950–9955.
[24] E.C. Hulme, GPCR activation: a mutagenic spotlight on crystal structures, Trends Pharmacol. Sci. 34 (2013) 67–84.
[25] M.C. Lagerström, J. Klovins, R. Fredriksson, D. Fridmanis, T. Haitina, M.K. Ling, M.M. Berglund, H.B. Schiöth, High affinity agonistic metal ion binding sites within the melanocortin 4 receptor illustrate conformational change of transmembrane region 3, J. Biol. Chem. 278 (2003) 51521–51526.
[26] W. Liu, j E. Chun, A.A. Thompson, P. Chubukov, F. Xu, V. Katritch, G.W. Han, C.B. Roth, L.H. Heitman, A.P. Ijzerman, V. Cherezov, R.C. Stevens, Structural basis for allosteric regulation of GCPRs by sodium ions, Science 337 (2012) 232–236.
[27] F. Delaglio, S. Grzesiek, G.W. Vuister, G. Zhu, J. Pfeifer, A. Bax, NMRPipe: a multidimensional spectral processing system based on UNIX pipes, J. Biomol. NMR 6 (1995) 277–293.
[28] T.D. Goddard, D.G. Kneller, SPARKY 3, University of California, San Francisco, CA, 2004.
[29] G.W. Vuister, A. Bax, Quantitative J correlation: a new approach for measuring homonuclear three bond J(HNHa) coupling constants in ^{15}N-enriched proteins, J. Am. Chem. Soc. 115 (1993) 7772–7777.
[30] S. Grzesiek, A. Bax, Improved 3D triple-resonance NMR techniques applied to a 31-kDa protein, J. Magn. Reson. 96 (1992) 432–440.
[31] J. Stonehouse, R.T. Clowes, G.L. Shaw, J. Keeler, E.D. Laue, Minimisation of sensitivity losses due to the use of gradient pulses in triple-resonance NMR of proteins, J. Biomol. NMR 5 (1995) 226–232.
[32] D.R. Muhandiram, L.E. Kay, Gradient-enhanced triple-resonance three-dimensional NMR experiments with improved sensitivity, J. Magn. Reson. 103 (1994) 203–216.
[33] M. Ikura, L.E. Kay, A. Bax, A novel approach for sequential assignment of 1H, 13C, and 15N spectra of proteins: heteronuclear triple-resonance three-dimensional NMR spectroscopy, application to calmodulin, Biochemistry 29 (1990) 4659–4667.
[34] A. Grzesiek, A. Bax, The origin and removal of artifacts in 3D HCACO spectra of proteins uniformly enriched with ^{13}C, J. Magn. Reson. 102 (1993) 103–106.
[35] L.E. Kay, G.Y. Xu, A.U. Singer, D.R. Muhandiram, J.D. Forman-Kay, A gradient-enhanced HCCH-TOCSY experiment for recording sidechain 1H and 13C correlations in H_2O samples of proteins, J. Magn. Reson. 101 (1993) 333–337.
[36] M. Piotto, V. Saudek, V. Sklenar, Gradient-tailored excitation for single-quantum NMR spectroscopy of aqueous solutions, FEBS Lett. 2 (1992) 661–665.
[37] A.L. Davis, J. Keeler, E.D. Laue, D. Moskau, Experiments for recording pureabsorption heteronuclear correlation spectra using pulsed field gradients, J. Magn. Reson. 98 (1992) 207–216.
[38] T. Herrmann, P. Guntert, K. Wuthrich, Protein NMR structure determination with automated NOE assignment using the new software CANDID and the torsion angle dynamics algorithm DYANA, J. Mol. Biol. 319 (2002) 209–227.
[39] G. Cornilescu, F. Delaglio, A. Bax, Protein backbone angle restraints from searching a database for chemical shift and sequence homology, J. Biomol. NMR 13 (1999) 289–302.
[40] R.A. Laskowski, J.A. Rullmannn, M.W. MacArthur, R. Kaptein, J.M. Thornton, AQUA and PROCHECK-NMR: programs for checking the quality of protein structures solved by NMR, J. Biomol. NMR 8 (1996) 477–486.
[41] W.L. DeLano, The PyMOL Molecular Graphics System, DeLano Scientific, San Carlos, CA, 2002.
[42] R. Koradi, M. Billeter, K. Wuthrich, MOLMOL: a program for display and analysis of macromolecular structures, J Mol Graphics 14 (1996) 29–32 (51-55).
[43] Desmond Molecular Dynamics System, Version 3.5, D. E. Shaw Research, New York, NY, 2013.
[44] Maestro-Desmond Interoperability Tools, Version 3.5, Schrödinger, New York, NY, 2013.
[45] Prime, version 3.5, Schrödinger, LLC, New York, NY, 2014.
[46] BioLuminate, Version 1.4, Schrödinger, LLC, New York, NY, 2014.
[47] Desmond Molecular Dynamics System, Version 3.7, D. E. Shaw Research, New York, NY, 2014.
[48] W. Liu, E. Chun, A.A. Thompson, P. Chubukov, F. Xu, V. Katritch, G.W. Han, C.B. Roth, L.H. Heitman, A.P. IJzerman, V. Cherezov, R.C. Stevens, Structural basis for allosteric regulation of GPCRs by sodium ions, Science 337 (2012) 232–236.
[49] K. Wuthrich, NMR structures of biological macromolecules, in: D.M. Grant, R.K. Harris (Eds.), Encyclopedia of Nuclear Magnetic Resonance, Wiley, New York, 1996, pp. 710–719.
[50] S. Yohannan, S. Faham, D. Yang, J.P. Whitelegge, J.U. Bowie, The evolution of transmembrane helix kinks and the structural diversity of G protein-coupled receptors, Proc. Natl. Acad. Sci. U. S. A. 27 (2004) 959–963.
[51] T. Cierpicki, I. Zhukov, R.A. Byrd, J. Otlewski, Hydrogen bonds in human ubiquitin reflected in temperature coefficients of amide protons, J. Magn. Reson. 157 (2002) 178–180.
[52] B.W. Cook, G.S. Shaw, Architecture of the catalytic HPN motif is conserved in all E2 conjugating enzymes, Biochem. J. 445 (2012) 167–174.
[53] C. Govaerts, A. Lefort, S. Costagliola, S.J. Wodak, J.A. Ballesteros, J. Van Sande, L. Pardo, G. Vassart, A conserved Asn in transmembrane helix 7 is an on/off switch in the activation of the thyrotropin receptor, J. Biol. Chem. 276 (2001) 22991–22999.
[54] O. Fritze, S. Filipek, V. Kuksa, K. Palczewski, K.P. Hofmann, O.P. Ernst, Role of the conserved NPxxY(x)5,6F motif in the rhodopsin ground state and during activation, Proc. Natl. Acad. Sci. U. S. A. 100 (2003) 2290–2295.
[55] K.J. Kohlhoff, D. Shukla, M. Lawrenz, G.R. Bowman, D.E. Konerding, D. Belov, R.B. Altman, V.S. Pande, Cloud-based simulations on Google Exacycle reveal ligand modulation of GPCR activatio0n pathways, Nat. Chem. 6 (2014) 15–21.
[56] K.L. Chapman, G.K. Kinsella, A. Cox, D. Donnelly, J.B.C. Findlay, Interactions of the melanocortin-4 receptor with the peptide agonist NDP-MSH, J. Mol. Biol. 401 (2010) 433–450.
[57] M.S. Johnson, D.N. Robertson, P.J. Holland, E.M. Lutz, R. Mitchell, Role of the conserved NPxxY motif of the 5-HT2A receptor in determining selective interaction with isoforms of ADP-ribosylation factor (ARF), Cell. Signal. 18 (2006) 1793–1800.
[58] S.S. Ericksen, D.F. Cummings, H. Weinstein, J.A. Schetz, Ligand selectivity of D2 dopamine receptors is modulated by changes in local dynamics produced by sodium binding, J. Pharmacol. Exp. Ther. 328 (2009) 40–54.
[59] J. Selent, F. Sanz, M. Pastor, G. De.Fabritiis, Induced effects of sodium ions on dopaminergic G-protein coupled receptors, PLoS Comput. Biol. 6 (2010) e1000884.
[60] H. Gutiérrez-de-Terán, A. Massink, D. Rodríguez, W. Liu, G.W. Han, J.S. Joseph, I. Katritch, L.H. Heitman, L. Xia, A.P. Ijzerman, V. Cherezov, V. Katritch, R.C. Stevens, The role of a sodium ion binding site in the allosteric modulation of the A2A adenosine G-protein-coupled receptor, Structure 21 (2013) 2175–2185.